

Scattering Theory of Chiral Edge Modes in Topological Magnon Insulators

Stefan Birnkammer,^{1,2} Michael Knap,^{1,2} Johannes Knolle,^{1,2,3} Alexander Mook,⁴ and Alvisе Bastianello^{1,2}

¹Department of Physics, Technical University of Munich, 85748 Garching, Germany

²Munich Center for Quantum Science and Technology (MCQST), Schellingstraße 4, 80799 München, Germany

³Blackett Laboratory, Imperial College London, London SW7 2AZ, United Kingdom

⁴Department of Physics, Johannes Gutenberg Universität Mainz, 55128 Mainz, Germany

(Dated: October 10, 2024)

Topological magnon insulators exhibit robust edge modes with chiral properties similar to quantum Hall edge states. However, due to their strong localization at the edges, interactions between these chiral edge magnons can be significant, as we show in a model of coupled magnon-conserving spin chains in an electric field gradient. The chiral edge modes remain edge-localized and do not scatter into the bulk, and we characterize their scattering phase: for strongly-localized edge modes we observe significant deviation from the bare scattering phase. This renormalization of edge scattering can be attributed to bound bulk modes resonating with the chiral edge magnons, in the spirit of Feshbach resonances in atomic physics. We argue a real-time measurement protocol using spin-polarized scanning tunneling spectroscopy to study their scattering dynamics. Our result show that interaction among magnons can be encoded in an effective edge model of reduced dimensionality, where the interactions with the bulk renormalize the effective couplings. This work paves the way to develop a many-body effective theory for chiral edge magnons.

Introduction – Quantum magnets with a topologically *trivial* ground state supporting topologically *nontrivial* spin excitations are an emerging platform to study the topology of collective excitations [1]. They are found in ordered magnets [2–14] and quantum paramagnets [15–19]. When time-reversal symmetry is broken, chiral spin excitations propagating along the boundaries of the sample are protected by the topology of the bulk, giving rise to the idea of topological magnonics [20–24]. Although direct experimental evidence for chiral edge spin excitations is yet to be achieved, transport [3, 25–27] and neutron scattering data [28–32] compatible with topological spin excitations have been reported. However, the stability against decay of topological magnon modes still needs to be firmly established [33–35]. The properties of magnon edge modes can be investigated by spin-polarized scanning tunneling spectroscopy (STS) through local excitation [36, 37]. While much of the focus thus far has been on investigating the properties of isolated edge excitations, many experimental setups operate in a regime where multiple edge modes are excited simultaneously. As they will interact with one another, it is an important open challenge to study the characteristics of scattering between edge modes. A positive answer would lay the groundwork for building an effective edge theory at the many-body level.

Herein, we show the stability of chiral magnons upon scattering and characterize their properties. We emphasize the critical role of the bulk spectrum in determining the interaction characteristics of edge states. Scattering of chiral magnons can be directly explored using spin-polarized STS through a real-time injection measurement protocol, as shown in Fig. 1 a): Chiral edge magnons with different velocities can be sequentially excited. As illustrated in Fig. 1 b), the interactions between edge modes are reflected in a scattering delay Δd , measured relative to the evolution of free particles. This delay can be extracted by monitoring the chiral excitations at a different position of the edge, see Fig. 1 a).

The model – We require both spin conservation and ferromagnetism to ensure the number of magnons is con-

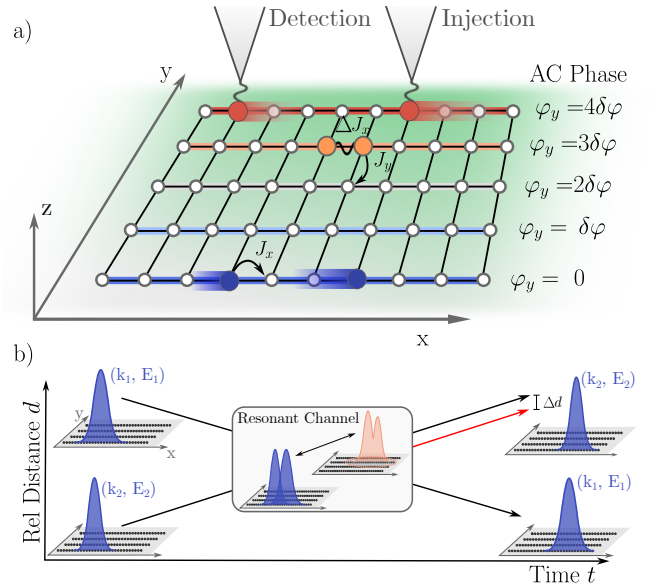


Figure 1. **Topological magnons in coupled wires.** a) Sketch of the model (1): we consider a two-dimensional system made of an array of spin-1/2 chains. The presence of a linear Aharonov-Casher (AC) phase induced by a constant electric field gradient in the y direction $\vec{E} = \Delta E \vec{y}$, gives rise to localized bulk modes and chiral edge modes. b) Cartoon scattering of two chiral magnons at the same edge. Our results demonstrate that the scattering of edge modes is elastic (no scattering into the bulk), but resonances with bulk modes strongly renormalize effective interactions, manifesting in a scattering shift Δd .

stant. We assume that any perturbation deviating from this condition—setting a finite timescale for the proposed scattering experiments—is small enough to be negligible. As a concrete example, we construct a two-dimensional system from exactly solvable one-dimensional XXZ spin chains with tunable magnon-magnon interactions [38–40]. The individual chains are arranged in the x - y plane, aligned parallel in the

x -direction, and labeled according to their equidistant positions along the y -axis, see Fig. 1 a). The Hamiltonian for the y -th chain takes the form

$$\mathcal{H}^{(y)} = -\frac{J_x}{2} \sum_x \left[\left(e^{-i\varphi_y} \sigma_{x,y}^+ \sigma_{x+1,y}^- + \text{h.c.} \right) + \Delta \sigma_{x,y}^z \sigma_{x+1,y}^z \right]. \quad (1)$$

The interactions between magnons are controlled by the anisotropy Δ , with magnons behaving as hardcore bosons in the limit $\Delta = 0$. To induce chiral edge modes, we use the Aharonov-Casher (AC) phase [41–46]: an electric field gradient causes a y -dependent phase $\varphi_y \propto \int_{(x,y)}^{(x+1,y)} d\vec{x} \cdot (\vec{E} \wedge \hat{e}_z) \equiv y\delta\varphi$ for the intra-chain hopping. We measure energy scales in units of the intra-wire hopping and hence set $J_x = 1$. The Hilbert space for Eq. (1) contains sectors with a definite number of magnons, and the single magnon spectrum is obtained by Fourier transformation. In the absence of any interchain coupling, the phase φ_y is equivalent to different gauges of lattice momenta, thus resulting in a global shift of the one-magnon bands $k \rightarrow k + \varphi_y$, see Fig. 2 a) (gray lines).

We now allow for tunneling between the chains leading to the full Hamiltonian

$$\mathcal{H} = \sum_y \mathcal{H}^{(y)} - J_y \sum_{x,y} \frac{1}{2} \left(\sigma_{x,y}^+ \sigma_{x,y+1}^- + \text{h.c.} \right). \quad (2)$$

A nonzero inter-wire hopping J_y causes level repulsion between the wires' energy bands, opening up a bulk gap in the system. Only the branches associated with the edge wires escape level repulsion in certain momenta regions $k \in [k_1, k_2]$, giving rise to localized chiral edge modes with dispersion $\varepsilon(k)$, and group velocity $v(k) \equiv \partial_k \varepsilon(k)$ [47]. In the thermodynamic limit, bulk modes become localized and have flat energy bands, while edge modes (i) have a well-defined chirality given by the sign of the group velocity, and (ii) are dispersive, i.e. $\partial_k v(k) \neq 0$; thus they scatter.

We show an example of the chiral spectrum in Fig. 2 a) for inter-wire hopping strength $J_y = 0.5$, and indicate the localization of individual magnon modes in the bulk by color coding according to Fig. 1 a), for $\delta\varphi = \frac{2\pi}{5}$. For the sake of consistency, we fix the AC phase to this value throughout the rest of this work, but generalization to other values of $\delta\varphi$ are straightforward and lead to similar results.

Real-time scattering of Chiral Magnons – When scattering channels into bulk modes or other edge bands are closed, the scattering remains effectively one-dimensional. As a result, due to energy and momentum conservation, two-magnon scattering is elastic, preserving the individual momenta. However, this does not translate into a trivial scattering event as interactions induce a *scattering shift* Δd , which represents the spatial delay of the interacting particles compared to the free propagation of wave packets. This delay provides a direct measure of the strength of interactions between excitations. We now investigate real-time scattering of edge modes using exact diagonalization in the two magnon subspace. The bulk-integrated magnon distribution $|\psi(x)|^2$ as a function of time is shown in Fig. 2 b). To confirm the absence of leakage into

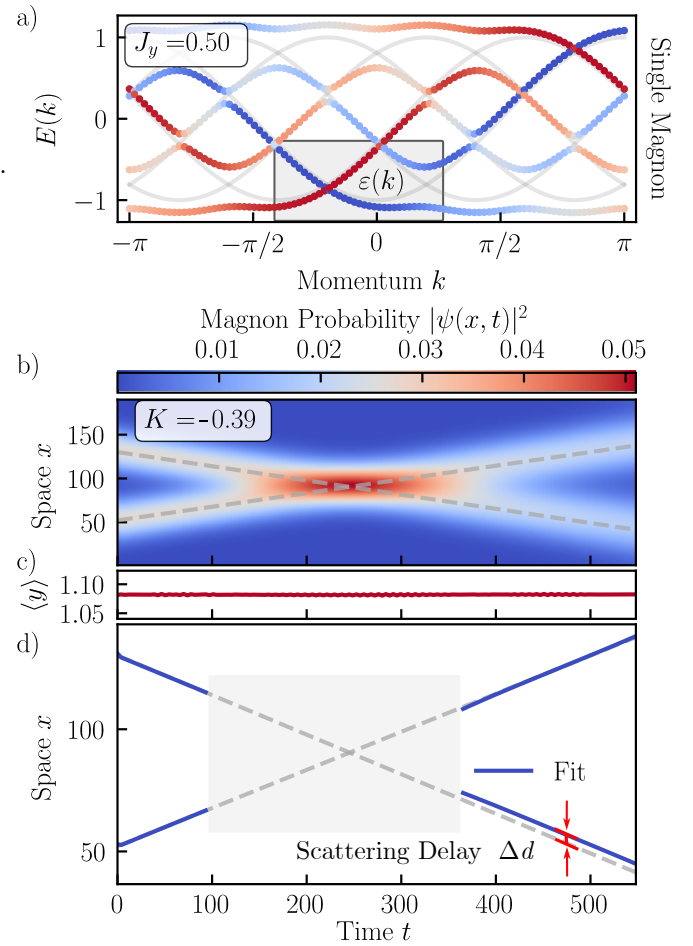


Figure 2. **Real time scattering of chiral magnons.** a) Single magnon spectrum with $\delta\varphi = 2\pi/5$ for the case of uncoupled wires, consisting of multiple copies of single-wire bands shifted in the momentum space (gray lines). Inter-wire hopping $J_y \neq 0$ gives band repulsion, and the spectrum shifts to stationary bulk modes and edge chiral states. b) Real-time simulation of a scattering event of two chiral magnons with total momentum $K = -0.39$ and relative momentum $q = -0.20$, and parameters $(J_y, \Delta) = (0.5, 0.8)$. We track the bulk-integrated magnon distribution $|\psi(x)|^2$, with x the relative distance. For a better visualization, we consider a comoving frame with the same velocity of the pair of magnons. The gray dashed lines are the trajectories of the initial position of the wavepackets, evolved with the initial velocities (free evolution). c) The state remains localized at the edge during the scattering, as shown in the average position in the transverse direction $\langle y \rangle$. d) We compare the free evolution (gray dashed line) with the peaks position (blue line), showing displacement after scattering.

bulk modes or transitions to other edge states during scattering, we compute the wave packets' average edge localization $\langle y \rangle$, which stays constant in time, see Fig. 2 c). In Fig. 2 d), we quantify the scattering shift Δd by comparing the actual peak positions (solid blue line) with those predicted for free propagation (dashed gray line). While this real-time scattering analysis provides a way to characterize the two-body problem at the edge, we will next develop a more efficient method to extract the scattering information encoded in Δd across a

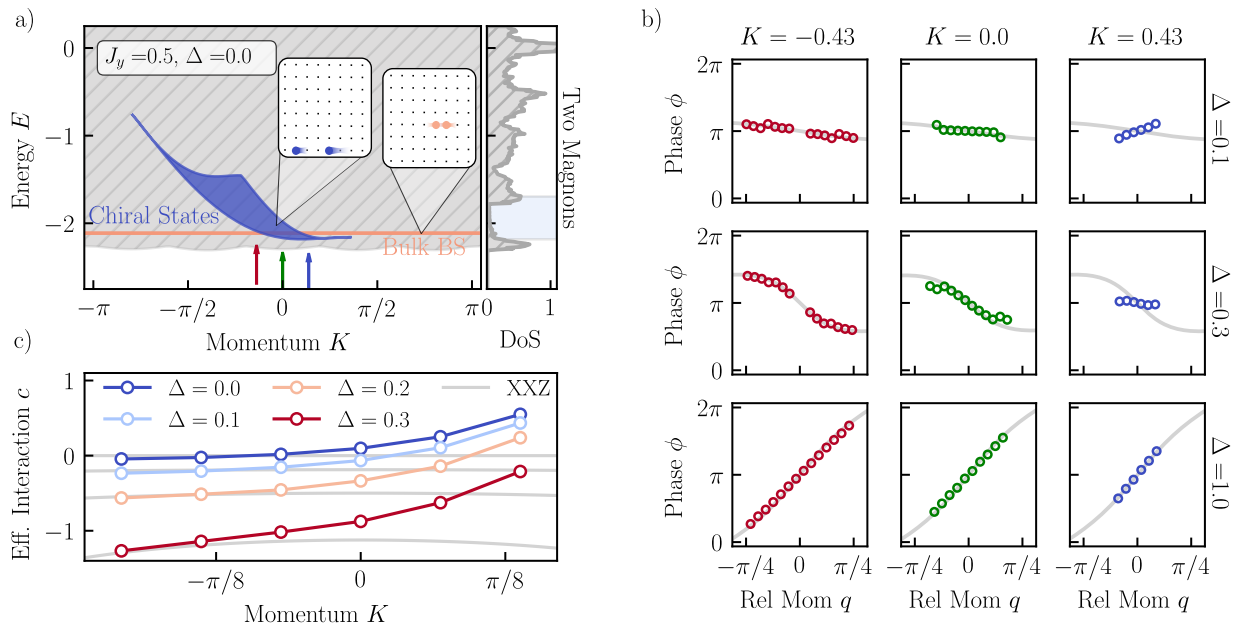


Figure 3. **Scattering phases.** a) Left: Allowed energy-momentum window for scattering magnons (blue) embedded in the two magnon continuum (gray area). Non-dispersive bulk bound modes with neighboring magnons (BS) are partially overlapping with the energy window of the asymptotic edge magnons (blue). The parameters are $(J_y, \Delta) = (0.5, 0.0)$. Right: Momentum-integrated density of states capturing the low density of states within the bulk gap (lightblue shaded region). b) Extracted scattering phases for asymptotic states of different relative momenta q for fixed total momenta $K \in \{-0.43, 0, 0.43\}$ (left, middle, right column) for different $\Delta \in \{0.1, 0.3, 1.0\}$. The one-dimensional XXZ prediction (gray line) is provided for comparison, highlighting a strong renormalization for positive K and small Δ . c) Comparison of effective interaction strength c extracted from the scattering phase and chiral dispersion for numerically extracted results and analytical predictions for one-dimensional XXZ result (gray lines).

broader parameter range. This approach will be contrasted against predictions from the standard XXZ theory on the edge wires.

Characterization of edge scattering phases – We directly extract the desired scattering information from the interacting two particle spectrum. First, we utilize translational invariance along the chain direction, allowing us to represent (2) in momentum space. We then focus on the two-magnon sector of the Hilbert space and diagonalize the Hamiltonian within each center-of-mass (COM) momentum sector K . An example of the momentum-resolved low-energy continuum spectrum is shown in Fig. 3 a) (gray shaded region) for parameters $J_y = 0.5, \Delta = 0$. The topological bulk gap is visible in the momentum-integrated density of states (right panel). For our scattering analysis, we concentrate on the energy-momentum region allowed for two chiral magnons localized at the lower edge, as highlighted by the blue shaded area in Fig. 3 a). The energy-momentum window $[E_1(K), E_2(K)]$ for such an asymptotic state of two edge magnons with momenta k_1 and k_2 is determined from the chiral magnon dispersion, i.e. $E_1(K) \leq \varepsilon(k_1) + \varepsilon(k_2) \leq E_2(K)$, with $k_1 + k_2 = K$. The relevant asymptotic states for total momentum K are generally described by a superposition of plane waves $\psi_K(x, y_1, y_2) \propto e^{i(k_1 - k_2)x/2} \bar{\psi}_{k_1}(y_1) \bar{\psi}_{k_2}(y_2) + e^{-i(k_1 - k_2)x/2} e^{i\phi(k_1, k_2)} \psi_{k_1}(y_2) \bar{\psi}_{k_2}(y_1)$ representing the real-space wave function for magnons with relative distance x in

wires y_1 and y_2 . In this representation, we ignore the trivial global phase contribution from the COM motion with momentum K . Fitting the actual wavefunction for a given total momentum K to this functional form allows us to extract the scattering phase ϕ as a function of the relative momentum $q = (k_1 - k_2)/2$ (see Supplementary Material for details). The scattering phase ϕ connects back to the real-time scattering results in Fig. 2 d) through its relation to the scattering shift, i.e. $\Delta d \propto \partial_{k_1} \phi(k_1, k_2)$ [48].

The scattering phase ϕ as a function of the relative momentum q at different total momenta K and anisotropies Δ are shown in Fig. 3 b) for interchain hopping $J_y = 0.5$. As chiral magnons are strongly localized and thus predominately live on the outmost chain, it is pertinent to compare their scattering properties with those of magnons in a single one-dimensional XXZ chain [40]. While in some cases this is a good approximation, for certain values of K and Δ we observe a strong renormalization. In particular, a comparison of the numerical results with analytical predictions for the one-dimensional XXZ chain at the edge (gray lines) reveals significant renormalization of the interacting theory at large momenta K and small anisotropies $\Delta \in \{0.1, 0.3\}$. In contrast, for small K or large Δ the results align well with the bare XXZ predictions. It is worth noting that we find real-valued ϕ only indicating that there is indeed no weight of the wavefunction transferred to the bulk during scattering.

To provide a more comprehensive comparison between the effective scattering theory and the bare XXZ model, we consider the momentum-dependent scattering length $a(k) \equiv \lim_{p \rightarrow k} \partial_p \phi(p, k)$ renormalized with the effective mass $m^*(k) \equiv (\partial_k^2 \varepsilon(k))^{-1}$, and define the interaction $c(k) \equiv -1/[m^*(k)a(k)]$. The parameter $c(k)$ represents the contact interaction in an effective one-dimensional edge Hamiltonian for two magnons with small relative momenta: see Supplementary Material for details. In Fig. 3 c) we show the effective interaction as a function of the COM momentum for different anisotropies, observing strong deviations from the bare XXZ for large and positive momenta. As we will demonstrate, the observed strong renormalization effects in the edge theory can be traced back to bound modes in the bulk, which can resonate with the chiral magnon pair.

Bulk Resonances – The energy of scattering edge states is determined by the one-magnon band and remains independent of Δ due to the large spatial separation between the two magnons of an asymptotic state. Bulk modes, however, can resonate with the scattering states. A sketch of the relevant nondispersing eigenstates, which describe two bulk magnons in close proximity and are thus strongly interacting, is shown in Fig. 3 a). Each chain contributes one strongly bound mode, which is highly sensitive to changes in the anisotropy Δ . As interactions increase, these modes are eventually pushed out of the two-particle continuum, forming stable bound states (see Supplementary Material for more details) [49, 50]. The strong renormalization of scattering properties can be understood by considering an asymptotic state of two chiral magnons with total (and relative) momentum K (q) within the continuum of scattering states, as illustrated in Fig. 4 a). As the anisotropy Δ increases, it lowers the energy of all bulk-bound modes, causing a series of resonances at interaction values $\Delta_1(K, q), \dots, \Delta_N(K, q)$. This effect strongly depends on the total momentum K of the asymptotic states: For small K , all relevant bulk modes are already situated at lower energies than the asymptotic energy window, even at $\Delta = 0$, as shown in Fig. 3 a). The situation is different though for large K .

The number of resonant bulk modes N is expected to remain finite also in the thermodynamic limit $L_y \rightarrow \infty$, as only bulk modes near the edges have significant overlap with edge modes. Once the highest-energy bulk mode moves out of resonance with the asymptotic continuum, edge scattering becomes well-described by the one-dimensional XXZ model, as seen in Fig. 3 b). We further illustrate this behavior in Fig. 4 b) - f), by examining how the characteristics of bulk-bound states change with varying Δ . As Δ decreases from strong interactions, the energy of certain bulk-bound states enters the two-chiral magnon continuum, allowing them to hybridize with edge states. This hybridization is detected through the edge participation factor $P = \sum_x |\psi(x, y = 1)|^2$, which shows three distinct peaks, signaling strong coupling with different asymptotic scattering states, as shown in Fig. 4 b) and c).

We then compare the unhybridized wave function, shown in Fig. 4 d), with its form at two of the most prominent resonances, as depicted in Fig. 4 e) and f). In all cases, the wave function remains sharply peaked at small relative distances x ,

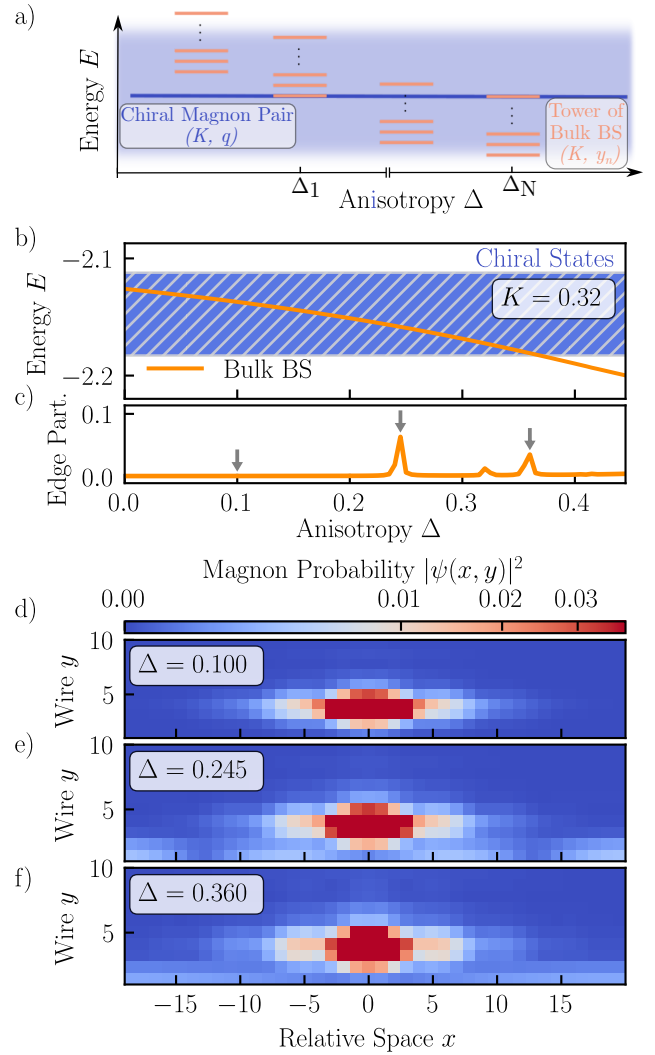


Figure 4. **Resonances.** a) Pictorial representation of scattering resonances. Upon changing Δ , a set of bulk BS bands of total momentum K gets tuned through a continuum of asymptotic states with variable relative momentum q , triggering resonances. b) Tracing one particular bound mode in the bulk of fixed total momentum $K = 0.32$ through the continuum (blue region) of asymptotic states yields resonances with different chiral states. c) This is resolved in the participation of the wavefunction at the edge. For our finite size simulations we find three resonance peaks. d) - f) Resonances of the bulk BS with asymptotic states are reflected in the magnon distribution $|\psi(x, y)|^2$ in relative space x and the bulk y . In contrast to the unhybridized case d) the wavefunction contains strong contributions from the edge at the resonances (e,f).

but at resonance, a plane wave profile emerges in the magnon distribution near the edge, indicating hybridization with scattering states. The resonances change the effective magnon interactions, which confirms the behavior seen in Fig. 3 c). Notably, when comparing the hybridized cases in Fig. 4 e) and f), additional nodes in the edge plane wave profile become apparent, which correspond to different relative momenta q of the hybridizing asymptotic states. As the system size increases

along the x -direction, the spectrum of asymptotic edge states becomes denser, characterized by a continuous range of relative momenta q . Consequently, discrete bulk modes are tuned through a continuum of edge modes. However, the extent of hybridization between bound bulk states and edge modes ultimately depends on the spatial overlap of their respective wavefunctions.

Discussion. – We have investigated the scattering of chiral edge magnons in a two-dimensional magnet subjected to an electric field gradient. By thoroughly analyzing the interactions among edge modes, we demonstrated their stability during scattering events and extracted their corresponding scattering phases. Much like Feshbach resonances in atomic physics, the scattering of chiral magnons is significantly renormalized through resonances with bulk modes. Our work opens the door to describing the many-body dynamics of edge modes within an effective one-dimensional framework, which in the two-magnons sector is governed by the effective Hamiltonian

$$\mathcal{H}_{2\text{-eff}} = \varepsilon(k_1) + \varepsilon(k_2) + U_{2\text{-eff}}(k_1, k_2), \quad (3)$$

where $U_{2\text{-eff}}(k_1, k_2)$ captures the effective interactions among the two chiral magnons of energies $\varepsilon(k_{1,2})$. The effective interaction $U_{2\text{-eff}}(k_1, k_2)$ is uniquely determined by the scattering phase $\phi(k_1, k_2)$ through methods from inverse scattering [51–53]. At coincident momenta, one recovers the effective interaction previously introduced $c(k) = U_{2\text{-eff}}(k, k)$, and Eq. (3) is mapped into the Lieb-Liniger model [54, 55] de-

scribing galilean bosons with contact interactions. A brief account for the effective Hamiltonian and its small momentum limit is reported in the Supplementary Material. It will be intriguing to use Eq. (3) as a building block for a full-fledged many-body effective description, and take advantage of both powerful analytical methods and advanced numerical techniques available in one dimension. Our study underscores the crucial influence of bulk spectra on the many-body behavior of edge states in topological magnon systems. It would be fascinating to observe the phenomenology we have presented in experiments, such as through the proposed injection-measurement protocol applied to topological magnon candidates such as CrI₃ [29].

Acknowledgements. – We acknowledge support from the Deutsche Forschungsgemeinschaft (DFG, German Research Foundation) under Germany’s Excellence Strategy–EXC–2111–390814868, TRR 360 – 492547816, DFG grants No. KN1254/1-2, KN1254/2-1, and DFG Emmy Noether Programme—Project No. 504261060, the European Research Council (ERC) under the European Union’s Horizon 2020 research and innovation programme (grant agreement No. 851161), as well as the Munich Quantum Valley, which is supported by the Bavarian state government with funds from the Hightech Agenda Bayern Plus.

Data and Informations availability. – Data, data analysis, and simulation codes are available upon reasonable request on Zenodo [56].

-
- [1] P. A. McClarty, Topological magnons: A review, *Annual Review of Condensed Matter Physics* **13**, 171–190 (2022).
- [2] H. Katsura, N. Nagaosa, and P. A. Lee, Theory of the thermal hall effect in quantum magnets, *Phys. Rev. Lett.* **104**, 066403 (2010).
- [3] Y. Onose, T. Ideue, H. Katsura, Y. Shiomi, N. Nagaosa, and Y. Tokura, Observation of the magnon hall effect, *Science* **329**, 297 (2010).
- [4] L. Zhang, J. Ren, J.-S. Wang, and B. Li, Topological magnon insulator in insulating ferromagnet, *Phys. Rev. B* **87**, 144101 (2013).
- [5] K. A. van Hoogdalem, Y. Tserkovnyak, and D. Loss, Magnetic texture-induced thermal hall effects, *Phys. Rev. B* **87**, 024402 (2013).
- [6] A. Mook, J. Henk, and I. Mertig, Magnon hall effect and topology in kagome lattices: A theoretical investigation, *Phys. Rev. B* **89**, 134409 (2014).
- [7] A. Mook, J. Henk, and I. Mertig, Edge states in topological magnon insulators, *Phys. Rev. B* **90**, 024412 (2014).
- [8] S. A. Owerre, A first theoretical realization of honeycomb topological magnon insulator, *J. Phys.: Condens. Matter* **28**, 386001 (2016).
- [9] S. K. Kim, H. Ochoa, R. Zarzuela, and Y. Tserkovnyak, Realization of the haldane-kane-mele model in a system of localized spins, *Phys. Rev. Lett.* **117**, 227201 (2016).
- [10] F.-Y. Li, Y.-D. Li, Y. B. Kim, L. Balents, Y. Yu, and G. Chen, Weyl magnons in breathing pyrochlore antiferromagnets, *Nature Communications* **7**, 10.1038/ncomms12691 (2016).
- [11] A. Mook, J. Henk, and I. Mertig, Tunable magnon weyl points in ferromagnetic pyrochlores, *Phys. Rev. Lett.* **117**, 157204 (2016).
- [12] A. Mook, J. Henk, and I. Mertig, Thermal hall effect in non-collinear coplanar insulating antiferromagnets, *Phys. Rev. B* **99**, 014427 (2019).
- [13] A. Mook, S. A. Díaz, J. Klinovaja, and D. Loss, Chiral hinge magnons in second-order topological magnon insulators, *Phys. Rev. B* **104**, 024406 (2021).
- [14] M. J. Karaki, X. Yang, A. J. Williams, M. Nawwar, V. Doan-Nguyen, J. E. Goldberger, and Y.-M. Lu, An efficient material search for room-temperature topological magnons, *Science Advances* **9**, 10.1126/sciadv.ade7731 (2023).
- [15] J. Romhányi, K. Penc, and R. Ganesh, Hall effect of triplons in a dimerized quantum magnet, *Nature Communications* **6**, 10.1038/ncomms7805 (2015).
- [16] P. A. McClarty, F. Krüger, T. Guidi, S. F. Parker, K. Refson, A. W. Parker, D. Prabhakaran, and R. Coldea, Topological triplon modes and bound states in a shastry–sutherland magnet, *Nature Physics* **13**, 736 (2017).
- [17] D. G. Joshi and A. P. Schnyder, F_2 topological quantum paramagnet on a honeycomb bilayer, *Phys. Rev. B* **100**, 020407 (2019).
- [18] D. Bhowmick and P. Sengupta, Weyl triplons in $\text{SrCu}_2(\text{BO}_3)_2$, *Phys. Rev. B* **104**, 085121 (2021).
- [19] P. d’Ornellas and J. Knolle, Kitaev-heisenberg model on the star lattice: From chiral majorana fermions to chiral triplons, *Physical Review B* **109**, 094421 (2024).
- [20] R. Shindou, R. Matsumoto, S. Murakami, and J.-i. Ohe, Topological chiral magnonic edge mode in a magnonic crystal, *Phys.*

- [Rev. B **87**, 174427 \(2013\)](#).
- [21] R. Shindou, J.-i. Ohe, R. Matsumoto, S. Murakami, and E. Saitoh, Chiral spin-wave edge modes in dipolar magnetic thin films, [Phys. Rev. B **87**, 174402 \(2013\)](#).
- [22] R. Shindou and J.-i. Ohe, Magnetostatic wave analog of integer quantum hall state in patterned magnetic films, [Phys. Rev. B **89**, 054412 \(2014\)](#).
- [23] X. S. Wang, Y. Su, and X. R. Wang, Topologically protected unidirectional edge spin waves and beam splitter, [Phys. Rev. B **95**, 014435 \(2017\)](#).
- [24] X. S. Wang, H. W. Zhang, and X. R. Wang, Topological magnonics: A paradigm for spin-wave manipulation and device design, [Phys. Rev. Applied **9**, 024029 \(2018\)](#).
- [25] T. Ideue, Y. Onose, H. Katsura, Y. Shiomi, S. Ishiwata, N. Nagaosa, and Y. Tokura, Effect of lattice geometry on magnon hall effect in ferromagnetic insulators, [Phys. Rev. B **85**, 134411 \(2012\)](#).
- [26] M. Hirschberger, R. Chisnell, Y. S. Lee, and N. P. Ong, Thermal hall effect of spin excitations in a kagome magnet, [Phys. Rev. Lett. **115**, 106603 \(2015\)](#).
- [27] P. Czajka, T. Gao, M. Hirschberger, P. Lampen-Kelley, A. Banerjee, N. Quirk, D. G. Mandrus, S. E. Nagler, and N. P. Ong, Planar thermal hall effect of topological bosons in the kitaev magnet α -rucl₃, [Nature Materials **22**, 36 \(2023\)](#).
- [28] R. Chisnell, J. S. Helton, D. E. Freedman, D. K. Singh, R. I. Bewley, D. G. Nocera, and Y. S. Lee, Topological magnon bands in a kagome lattice ferromagnet, [Phys. Rev. Lett. **115**, 147201 \(2015\)](#).
- [29] L. Chen, J.-H. Chung, B. Gao, T. Chen, M. B. Stone, A. I. Kolesnikov, Q. Huang, and P. Dai, Topological spin excitations in honeycomb ferromagnet cr₁₃, [Phys. Rev. X **8**, 041028 \(2018\)](#).
- [30] L. Chen, J.-H. Chung, M. B. Stone, A. I. Kolesnikov, B. Winn, V. O. Garlea, D. L. Abernathy, B. Gao, M. Augustin, E. J. G. Santos, and P. Dai, Magnetic field effect on topological spin excitations in cr₁₃, [Phys. Rev. X **11**, 031047 \(2021\)](#).
- [31] F. Zhu, L. Zhang, X. Wang, F. J. dos Santos, J. Song, T. Mueller, K. Schmalzl, W. F. Schmidt, A. Ivanov, J. T. Park, J. Xu, J. Ma, S. Lounis, S. Blügel, Y. Mokrousov, Y. Su, and T. Brückel, Topological magnon insulators in two-dimensional van der waals ferromagnets CrSiTe₃ and CrGeTe₃: Toward intrinsic gap-tunability, [Science Advances **7**, eabi7532 \(2021\)](#).
- [32] M. dos Santos Dias, N. Biniskos, F. Dos Santos, K. Schmalzl, J. Persson, F. Bourdarot, N. Marzari, S. Blügel, T. Brückel, and S. Lounis, Topological magnons driven by the dzyaloshinskii-moriya interaction in the centrosymmetric ferromagnet mn₅ge₃, [Nature Communications **14**, 7321 \(2023\)](#).
- [33] P. A. McClarty, X.-Y. Dong, M. Gohlke, J. G. Rau, F. Pollmann, R. Moessner, and K. Penc, Topological magnons in Kitaev magnets at high fields, [Phys. Rev. B **98**, 060404 \(2018\)](#).
- [34] S. Koyama and J. Nasu, Flavor-wave theory with quasiparticle damping at finite temperatures: Application to chiral edge modes in the kitaev model, [Phys. Rev. B **108**, 235162 \(2023\)](#).
- [35] J. Habel, A. Mook, J. Willsher, and J. Knolle, Breakdown of chiral edge modes in topological magnon insulators, [Physical Review B **109**, 024441 \(2024\)](#).
- [36] J. Feldmeier, W. Natori, M. Knap, and J. Knolle, Local probes for charge-neutral edge states in two-dimensional quantum magnets, [Phys. Rev. B **102**, 134423 \(2020\)](#).
- [37] E. J. König, M. T. Randeria, and B. Jäck, Tunneling spectroscopy of quantum spin liquids, [Phys. Rev. Lett. **125**, 267206 \(2020\)](#).
- [38] W. Heisenberg, Zur Theorie des Ferromagnetismus, [Zeitschrift für Physik **49**, 619 \(1928\)](#).
- [39] H. Bethe, Zur theorie der metalle: I. eigenwerte und eigenfunktionen der linearen atomkette, [Zeitschrift für Physik **71**, 205 \(1931\)](#).
- [40] M. Takahashi, *Thermodynamics of one-dimensional solvable models* (Cambridge University Press, 2005).
- [41] T. Liu and G. Vignale, Electric control of spin currents and spin-wave logic, [Phys. Rev. Lett. **106**, 247203 \(2011\)](#).
- [42] F. Meier and D. Loss, Magnetization transport and quantized spin conductance, [Phys. Rev. Lett. **90**, 167204 \(2003\)](#).
- [43] K. Nakata, P. Simon, and D. Loss, Wiedemann-franz law for magnon transport, [Phys. Rev. B **92**, 134425 \(2015\)](#).
- [44] K. Nakata, S. K. Kim, J. Klinovaja, and D. Loss, Magnonic topological insulators in antiferromagnets, [Phys. Rev. B **96**, 224414 \(2017\)](#).
- [45] Y. Aharonov and A. Casher, Topological quantum effects for neutral particles, [Phys. Rev. Lett. **53**, 319 \(1984\)](#).
- [46] A. Mook, B. Göbel, J. Henk, and I. Mertig, Taking an electron-magnon duality shortcut from electron to magnon transport, [Phys. Rev. B **97**, 140401 \(2018\)](#).
- [47] T. Meng, Coupled-wire constructions: a luttinger liquid approach to topology, [The European Physical Journal Special Topics **229**, 527 \(2020\)](#).
- [48] E. P. Wigner, Lower limit for the energy derivative of the scattering phase shift, [Phys. Rev. **98**, 145 \(1955\)](#).
- [49] X. Qin, F. Mei, Y. Ke, L. Zhang, and C. Lee, Topological magnon bound states in periodically modulated heisenberg xxz chains, [Phys. Rev. B **96**, 195134 \(2017\)](#).
- [50] X. Qin, F. Mei, Y. Ke, L. Zhang, and C. Lee, Topological invariant and cotranslational symmetry in strongly interacting multi-magnon systems, [New Journal of Physics **20**, 013003 \(2018\)](#).
- [51] V. E. Korepin, N. M. Bogoliubov, and A. G. Izergin, *Quantum Inverse Scattering Method and Correlation Functions*, 1st ed. (Cambridge University Press, 1993).
- [52] N. A. Khokhlov and V. A. Knyr, Reconstruction of the optical potential from scattering data, [Phys. Rev. C **73**, 024004 \(2006\)](#).
- [53] V. I. Kukulin, V. N. Pomerantsev, and J. c. v. Horáček, Reconstruction of the potential from scattering data, [Phys. Rev. A **42**, 2719 \(1990\)](#).
- [54] E. H. Lieb and W. Liniger, Exact Analysis of an Interacting Bose Gas. I. The General Solution and the Ground State, [Physical Review **130**, 1605 \(1963\)](#).
- [55] E. H. Lieb, Exact Analysis of an Interacting Bose Gas. II. The Excitation Spectrum, [Physical Review **130**, 1616 \(1963\)](#).
- [56] S. Birnkammer, J. Knolle, M. Knap, A. Mook, and A. Bastianello, Scattering theory of chiral edge modes in topological magnon insulators, [Zenodo **10.5281/zenodo.13895647** \(2024\)](#).

Supplementary Information
 Scattering Theory of Chiral Edge Modes in Topological Magnon Insulators
 Stefan Birnkammer, Johannes Knolle, Michael Knap, Alexander Mook and Alvis Bastianello

1. THE STRONG ANISOTROPY LIMIT – CHIRAL MAGNON BOUND STATES

In the main text we emphasized how strongly bound eigenstates can be tuned through resonances with individual asymptotic chiral states. Having increased the bare interaction strength Δ to sufficiently large values these strongly localized modes will transition to form stable bound modes, separated in energy from the two-particle continuum, as shown in Fig. S1 a). In total a number of L_y bound state bands will experience this effect resembling the results for the single magnon spectrum. Each bound state band, however, is associated with twice the shift in momentum space. This is a result of the AC phase coupling to the physical spin charge of the excitation, the latter is double for the bound state compared to individual magnon excitations. In the spirit of the single magnon spectrum sufficient coupling between the wires, nonetheless, opens a bulk gap stabilizing two chiral bound state modes at the edges of the system, see Fig. S1 b) - d). Same as the single magnon edge modes these edge bound states are stable throughout the tested parameter regime. This is consistent with findings from Ref. [49, 50].

2. CHARACTERIZATION OF THE MANY-BODY THEORY OF EDGE MODES

1. Numerical Extraction of Scattering Phases

Our investigations on the edge theory in the main text are primarily based on the momentum dependent analysis of scattering phases. For this, we rely on a protocol consisting of the following points to extract scattering information from the numerically obtained spectra, also summarized in Fig. S1 e).

1. Determine the momentum-dependent energy window $[E_1(K), E_2(K)]$ possible for pairs of chiral magnons from the single magnon spectrum.
2. Diagonalize the two magnon Hamiltonian in the corresponding total momentum sector K .
3. Filter the eigenspectrum for the eigenenergies within $[E_1(K), E_2(K)]$.
4. Filter for asymptotic states described by a plane wave ansatz of the form $\psi(x, y_1, y_2) = A_{y_1, y_2} e^{iqx} + B_{y_1, y_2} e^{-iqx}$ in the limit $x \gg 1$ for every pair of wire indices (y_1, y_2) , checking for agreement between various y_1, y_2 .
5. From the fitted parameters q, A, B compute the scattering matrix $S(q) = \frac{B}{A}$ as a function of relative momentum q .

To increase the number of data points we additionally make use of properties under exchange of the scattering partners in the problem. Particle exchange results in a parity operation acting on the relative momentum $q \mapsto -q$, while leaving the center of mass momentum K unaltered. The scattering element S gets thereby mapped to its own inverse $S \mapsto S^{-1}$. We compare the extracted results against the analytical prediction for a XXZ spin chain taken from Ref. [40],

$$S_{\text{XXZ}}(K, q) = e^{i\phi_{\text{XXZ}}(K, q)} \quad \text{with} \quad \phi_{\text{XXZ}}(K, q) = \pi - i \log \left[\frac{1 - 4\Delta e^{i(\frac{K}{2} + q)} + e^{iK}}{1 - 4\Delta e^{i(\frac{K}{2} - q)} + e^{iK}} \right]. \quad (\text{S1})$$

A comparison between the XXZ predicted (bottom row) and the numerically extracted (top row) scattering phases ϕ is shown in Fig. S1 f) - h) for anisotropies $\Delta \in [0.0, 0.4, 1.0]$. We collect scattering phases for values of $K \in [-\frac{\pi}{4}, \frac{\pi}{4}]$ and show the results as a function of the localization length ℓ of the eigenstates. To further discriminate the individual data points we highlight their relative momenta via color coding. Strongest deviations appear at small Δ for less localized states. This fits the semiclassical expectation of two more delocalized edge states having a reduced chance of scattering during their orbital motion at the boundary. In reality this enhanced leaking into the bulk, however, abets hybridization with bulk modes and the existence of resonances.

In the main text we also extract the effective interaction for the scattering phase data. For this, we determine the slope of $\phi(q)$ in the linear regime around relative momenta $q = 0$. We correct the results by additionally weighting them with the effective magnon mass m^* obtained from the curvature of the single magnon dispersion, i.e. $m^*(K) = \frac{1}{\partial_K^2 \varepsilon(K)}$. The result quantifies

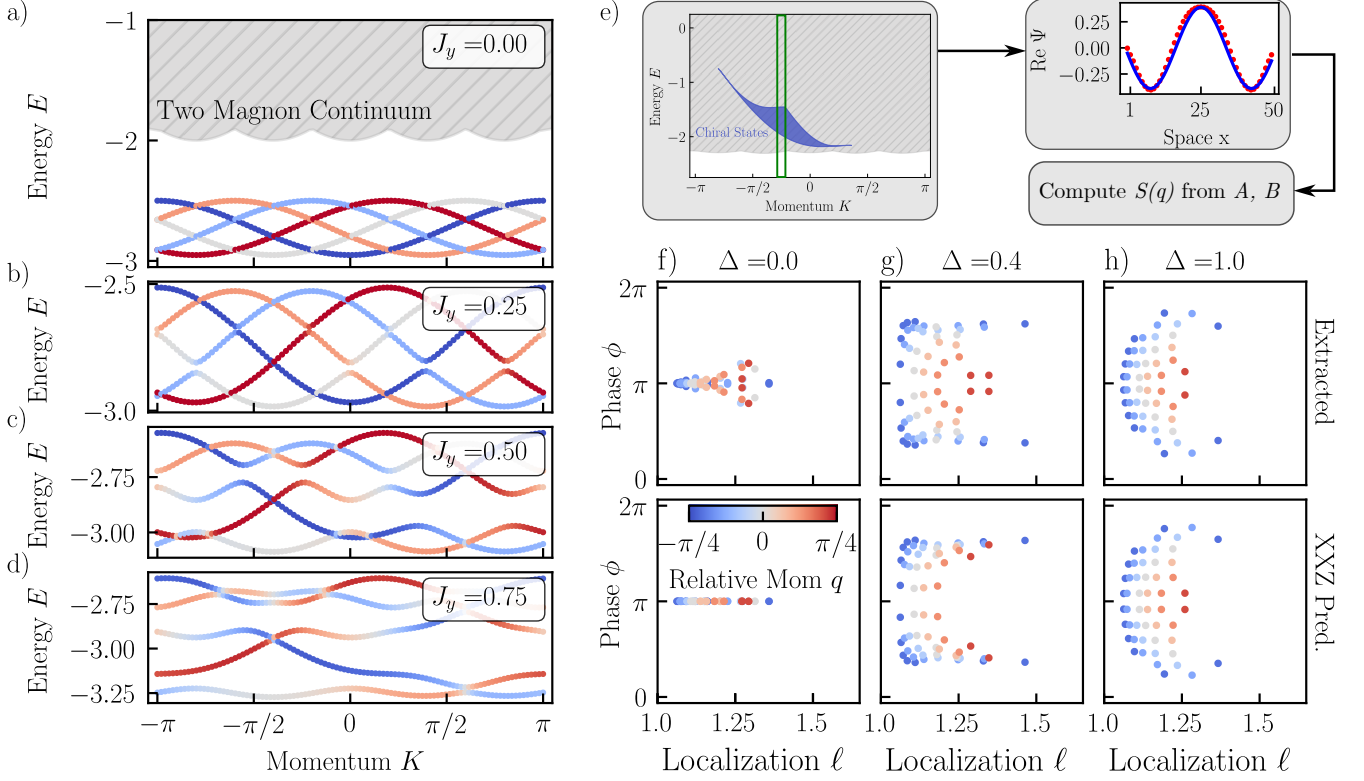


Figure S1. **Chiral Bound States and Scattering Phase Analysis.** a) Bound state bands separated in energy from the two magnon continuum for anisotropy $\Delta = 1.25$ and uncoupled wires. b) - d) Increasing hopping strength between the wires $J_y \in \{0.25, 0.50, 0.75\}$ opens a bulk gap and stabilizes modes of chiral bound states. e) Analysis of the scattering phase consists of (1.) - (3.) selecting eigenstates within the chiral energy window for a given momentum sector K , (4.) fitting the states against a plane wave ansatz and (5.) compute the scattering matrix S . f) - h) Comparison of extracted (top row) and XXZ predicted (bottom row) scattering phases for different K momenta and anisotropies $\Delta \in \{0.0, 0.4, 1.0\}$. The associated relative momenta are highlighted by color coding. Deviations are evident at low momenta ($\Delta = 0.0$) and especially for less localized states.

the one-dimensional scattering problem yielding the inverse product of effective magnon mass and the scattering length a for the edge theory, which is described in the next section. To quantify deviations from the bare XXZ theory we extract the same quantity from the analytical XXZ scattering prediction (S1)

$$c(K) = \left[-\frac{1}{m^*a} \right] (K) = \frac{4\Delta \cos(K)}{2\Delta - \cos\left(\frac{K}{2}\right)}. \quad (\text{S2})$$

The results summarize previous findings in a concise way; large (positive) momenta K are associated with a strongly interacting edge theory while small (negative) momenta follow the bare XXZ prediction.

2. Effective Theory on the Edge

In the main text we mention the possibility of constructing an effective one-dimensional edge theory for the scattering magnons from the knowledge of the scattering phase. In this section we present some further details for clarity. Since chiral edge modes remain confined in the lowest band, we can effectively project the Hamiltonian within this subspace, and introduce the effective two-particle Hamiltonian

$$\mathcal{H}_{2\text{-eff}} = \varepsilon(k_1) + \varepsilon(k_2) + U_{2\text{-eff}}(k_1, k_2), \quad (\text{S3})$$

where $U_{2\text{-eff}}(k_1, k_2)$ captures the effective interactions among the two chiral magnons of energies $\varepsilon(k_{1,2})$. The effective one-dimensional theory must lead to the same scattering events of the full two-dimensional scattering; this condition uniquely fixes

$U_{2\text{-eff}}(k_1, k_2)$ [52, 53].

The input of this program is the scattering phase extracted from numerical data as denoted in Section 2.1: The scattering phase $\phi(k_1, k_2)$ vanishes for non-interacting particles, and approaches π for hard-core bosons; for truly interacting cases, it has a non-trivial momentum dependence. Indeed, its momentum-derivative $\partial_{k_1}\phi(k_1, k_2)$ directly connects to the displacement observed after scattering [48].

The determination of the effective interactions $U_{2\text{-eff}}$ from the scattering phase $\phi(K, q)$ is the celebrated inverse scattering problem [51]: the solution is unique, and can be numerically found evaluating the Gel'fand-Levitan-Marchenko's equations [52] or solving an optimization problem based on chosen trial potentials [53]. Instead of aiming for a full characterization of the effective interactions we can, however, focus on the emergent theory in the assumption that the momenta of the scattering magnons belong to a small shell $k \in I_p \equiv [p - \delta p, p + \delta p]$. In this approximation, we Taylor expand the dispersion law

$$\varepsilon(k_{1,2}) \simeq \varepsilon(p) + v(p)(k_{1,2} - p) + \frac{1}{2m^*(p)}(k_{1,2} - p)^2 + \mathcal{O}((k_{1,2} - p)^3), \quad (\text{S4})$$

and approximate the interaction $U_{2\text{-eff}}(k_1, k_2) \simeq U_{2\text{-eff}}(p, p)$. Within this approximation, it is easy to convert $H_{2\text{-eff}}$ into a real space Hamiltonian, where the spatial coordinates $x_{1,2}$ conjugated to the small momenta shift $k_{1,2} - p$ are approximated as continuous

$$\Delta\mathcal{H}_{2\text{-eff}} \simeq -\frac{1}{2m^*(p)}(\partial_{x_1}^2 + \partial_{x_2}^2) + iv(p)(\partial_{x_1} + \partial_{x_2}) + c(p)\delta(x_1 - x_2), \quad (\text{S5})$$

where $\Delta\mathcal{H}_{2\text{-eff}} = \mathcal{H}_{2\text{-eff}} - 2\varepsilon(p)$ and $c(p) \equiv U_{2\text{-eff}}(p, p)$. The Hamiltonian (S5) describes the two-particle sector of the Lieb-Liniger (LL) model [54, 55]: with a contact potential, in a moving frame with velocity $v(p)$. The scattering phase of this model is $\phi_{\text{LL}}(k_1, k_2) = -2 \arctan\left(\frac{k_1 - k_2}{m^*(p)c(p)}\right)$ [54, 55]: by comparing the true scattering phase with the effective one, we can determine the effective interaction. Since we are within a small relative momentum approximation, we fix the effective interaction $c(p)$ through the scattering length $a(p) \equiv \lim_{k_1 \rightarrow p} \partial_{k_1}\phi(k_1, p)$, and the LL correspondence $a(p) = -1/(m^*(p)c(p))$.